Altered Orientation of Active Site Residues in Variants of Human Ferrochelatase. Evidence for a Hydrogen Bond Network Involved in Catalysis†

Harry A. Dailey,*,‡,§ Chia-Kuei Wu,§ Peter Horanyi,§ Amy E. Medlock,‡,§ Wided Najahi-Missaoui,§ Amy E. Burden,§ Tamara A. Dailey,‡,§ and John Rose§

Biomedical and Health Sciences Institute, Department of Biochemistry and Molecular Biology, Department of Microbiology, Paul D. Coverdell Center, University of Georgia, Athens, Georgia 30602

Received January 24, 2007; Revised Manuscript Received April 26, 2007

ABSTRACT: Ferrochelatase catalyzes the terminal step in heme biosynthesis, the insertion of ferrous iron into protoporphyrin to form protoheme IX. The crystal structures of human ferrochelatase both with and without the protoporphyrin substrate bound have been determined previously. The substrate-free enzyme has an open active site pocket, while in the substrate-bound enzyme, the active site pocket is closed around the porphyrin macrocycle and a number of active site residues have reoriented side chains. To understand how and why these structural changes occur, we have substituted three amino acid residues (H263, H341, and F337) whose side chains occupy different spatial positions in the substrate-free versus substrate-bound ferrochelatases. The catalytic and structural properties of ferrochelatases containing the amino acid substitutions H263C, H341C, and F337A were examined. It was found that in the H263C and H341C variants, but not the F337A variant enzymes, the side chains of N75, M76, R164, H263, F337, H341, and E343 are oriented in a fashion similar to what is found in ferrochelatase with the bound porphyrin substrate. However, all of the variant forms possess open active site pockets which are found in the structure of porphyrin-free ferrochelatase. Thus, while the interior walls of the active site pocket are remodeled in these variants, the exterior lips remain unaltered in position. One possible explanation for this collective reorganization of active site side chains is the presence of a hydrogen bond network among H263, H341, and E343. This network is disrupted in the variants by alteration of H263C or H341C. In the substrate-bound enzyme, the formation of a hydrogen bond between H263 and a pyrrole nitrogen results in disruption of the network. The possible role of this network in catalysis is discussed.

Ferrochelatase (protoheme ferrolyase, EC 4.99.1.1) catalyzes the terminal step in protoheme biosynthesis, the insertion of ferrous iron into protoporphyrin IX (*1*). This enzyme was the first protein identified and characterized whose catalytic role is the insertion of a metal ion into an organic molecule (*2*). The enzyme is widely distributed in nature, and while it is clearly similar in structure and gross catalytic properties among all sources, there is less than 10% sequence identity between the enzyme in higher eukaryotes and bacteria (*3*, *4*). At present, there are published crystal structures for three ferrochelatases: one bacterial (*5*), one yeast (*6*), and human (*7*). While these three protein structures are clearly related, they differ in that the *Bacillus subtilis* enzyme is a soluble monomeric protein and the eukaryotic enzymes are both inner mitochondrial membrane-associated homodimers. Animal and a few bacterial ferrochelatases also possess a [2Fe-2S] cluster (*4*, *8*, *9*), while the *Saccharomyces cerevisiae* and *B. subtilis* ferrochelatases do not.

Properties of the enzyme have been reviewed recently (*1*). The overall proposed enzymatic reaction involves iron acquisition and desolvation, followed by porphyrin binding, macrocycle distortion prior to removal of two pyrrolic protons, and finally metal chelation. While there is general acceptance that metalation is facilitated by macrocycle distortion, there is controversy about the stereochemistry of metalation, and no clear understanding of the catalytic mechanism. For each of the three ferrochelatases listed above, structures with bound putative substrate metals exist (*6*, *7*, *10*). For the bacterial enzyme, there is also a structure with *N*-methylmesoporphyrin, a tight binding, competitive inhibitor of ferrochelatase (*11*), along with the metal copper (*12*) and a structure of the enzyme with bound iron (*13*). No published structures are currently available for the bacterial enzyme with bound protoporphyrin IX or protoheme IX.

Recently, the first structure of any ferrochelatase with bound protoporphyrin IX substrate was determined (*14*). This substrate-bound human ferrochelatase differs substantially from the substrate-free human enzyme in two ways. First, the active site pocket, or "mouth", is closed around the porphyrin macrocycle, leaving only a small open hole over one pyrrole ring. Second, a select set of active site residues

† This work was supported by Grant DK32303 from the National Institutes of Health to H.A.D. J.R. and P.H. were supported by Grant GM62407.

* To whom correspondence should be addressed. Phone: (706) 542-2690. E-mail: hdailey@uga.edu.

‡ Biomedical and Health Sciences Institute, Department of Microbiology, and Paul D. Coverdell Center.

§ Department of Biochemistry and Molecular Biology.

10.1021/bi700151f CCC: $37.00
Published on Web 06/14/2007

Table 1: Statistics from the Crystallographic Analysis

	H263C/R115L	H341C/R115L	F337A/R115L
space group	$P2_12_12_1$	$P2_12_12_1$	$P2_12_12_1$
a (Å)	93.42	94.05	88.69
b (Å)	87.73	97.61	94.05
c (Å)	109.58	110.63	113.27
data analysis			
wavelength (Å)	1.5418	1.5418	1.0000
ϕ step (deg)	1.0	1.0	0.5
total rotation (deg)	360	360	200
data processing	HKL 1.9.1	HKL 1.9.1	HKL2000
R_{sym}	0.065	0.068	0.048
refinement statistics			
program	CNS 1.0	CNS 1.0	REFMAC 5.4
resolution (Å)	19.90−2.20	18.08−2.20	43.44−2.35
completeness[a] (%)	96.3 (90.1)	87.8 (56.9)	96.36 (97.9)
R_{cryst}[a]	0.209 (0.242)	0.210 (0.222)	0.195 (0.200)
R_{free}[a]	0.240 (0.272)	0.245 (0.290)	0.253 (0.309)
rmsd from ideality			
bond lengths (Å)	0.005	0.006	0.016
bond angles (deg)	1.2	1.2	1.8
Ramachandran analysis (*32*)[b]			
most favored region (%)	92.0 (99.7)	92.8 (99.3)	91.3 (99.7)
disallowed region (%)	0.3	0.3	0.3
final model			
residues	65−423	65−423	65−423
solvent atoms	308	426	342
detergent molecules	3	3	3
Cα deviations[c] (Å)	0.210	0.221	0.261
PDB entry	2PO5	2PO7	2PNJ

[a] Outer shell values in parentheses. [b] PROCHECK percent in all allowed regions shown in parentheses. [c] The root-mean-square deviations (Cα) between the 1HRK structure and the variant structure.

possess an altered spatial orientation in comparison to the substrate-free enzyme.

In this study, three active site residues have been altered by site-directed mutagenesis and the structures and kinetic properties of these variant forms of human ferrochelatase have been examined. The data demonstrate that reorientation of active site residues and closing of the active site are separable events. Furthermore, reorientation of active site residues occurs in a concerted manner that appears to involve a complex hydrogen bond network. It is proposed that realignment of this hydrogen bond network is the initial catalytic trigger that is necessary but not sufficient for macrocycle distortion.

MATERIALS AND METHODS

Recombinant human ferrochelatase was produced and purified as previously described (*15*). All studies reported herein employ an R115L variant of human ferrochelatase that has normal activity and has had its crystallographic structure determined previously (*7*). Production of recombinant human ferrochelatase H263C and H341C variants has been described previously (*15*). The N75A, M76A, and F337A variants were produced and verified using the same previously described techniques (*16*).

Enzyme assays were performed using a continuous direct spectroscopic assay (*17*) at 25 °C. Kinetic parameters were determined from data sets of 10 assays.

Structure Determination. Crystals of the H263C/R115L and H341C/R115L variants were obtained using conditions published for the R115L variant (*16*) with seeding. Crystals for the F337A variant were grown by the microbatch under oil (70:30 paraffin/silicone oil mixture) method using 2 μL drops containing equal volumes of protein solution [64 mg/mL in 50 mM Tris MOPs, 0.1 M KCl, 1% sodium cholate, and 250 mM imidazole (pH 8.1)] and precipitant solution [0.2 M sodium acetate trihydrate and 0.1 M sodium cacodylate (pH 6.5) in 30% (w/v) polyethylene glycol 8000 (Hampton Crystal Screen I-28, Hampton Research]. The drops were incubated at 18°C, and crystals suitable for mounting were observed after 4 days.

Crystals for the H263C/R115L, H341C/R115L, and F337A/R115L variants were harvested and mounted using the loop mounting technique of Teng (*18*) and flash-frozen in liquid nitrogen. No cryoprotection was necessary.

For the H263C/R115L and H341C/R115L variants, data were collected under cryogenic conditions ($T = 100$ K) on an Raxis IV image plate detector using mirror-focused (MSC Blue confocal optics) 5 kW X-rays. The data were indexed, integrated, and scaled using HKL version 1.9.1 (*19*). For the F337A/R115L variant, data were collected under cryogenic conditions ($T = 105$ K) on beamline 22BM (SER-CAT) of the Advanced Photon Source (Argonne National Laboratory, Argonne, IL) using a MarResearch 225 CCD detector. The resulting data were indexed, integrated, and scaled using the HKL2000 program suite (*19*). Data collection and processing details are collected in Table 1.

The structures of the H263C/R115L, H341C/R115L, and F337A/R115L variants were determined by difference Fourier analysis since the crystals were isomorphous with those of the R115L variant whose structure (PDB entry 1HRK) has been previously reported (*7*). Refinement of the variant structures was carried out using CNS (*20*) for the H263C/R115L and H341C/R115L variants, and REFMAC (*21*) was used for the F337A/R115L variant, together with manual model adjustment using XFIT (*22*) when needed. Refinement statistics for the three structures are collected in Table 1.

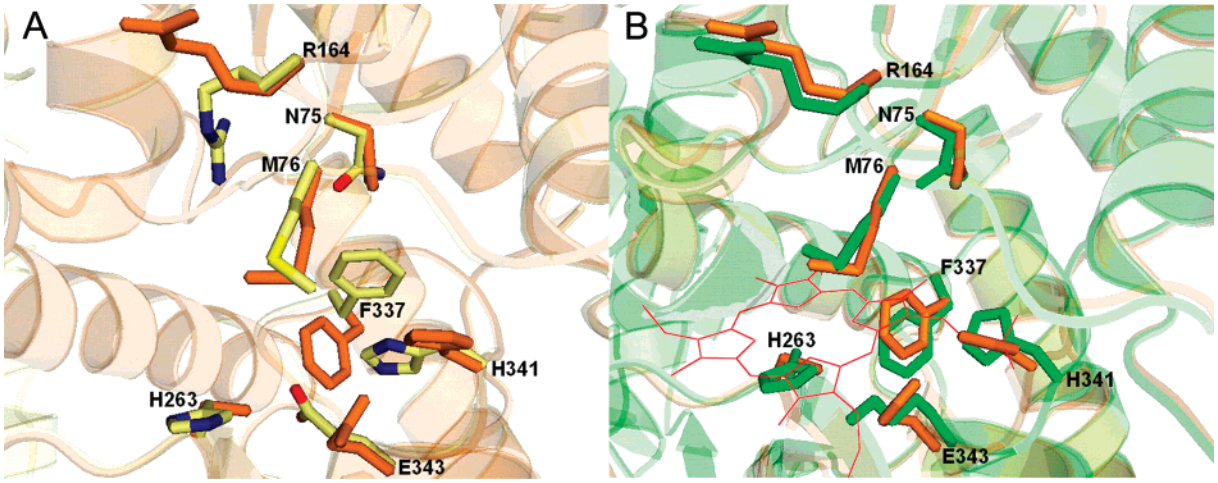

FIGURE 1: Reorientation of active site residues. (A) The orientations of select active site residues in the wild type and the H263C variant form of human ferrochelatase are pictured. The view into the active site shows the orientation of the side chains of N75, M76, R164, H263, F337, H341, and E343. The wild-type enzyme is colored cream, red, blue, and yellow for carbon, oxygen, nitrogen, and sulfur atoms (PDB entry 1HRK), respectively, and the H263C variant is colored orange. (B) The orientations of select active site resides of the substrate-bound (E343K variant) and H263C variant forms of human ferrochelatase are illustrated. A view of the active site shows the similarity in the orientation of specific active site residues, including N75, M76, R164, H263, H341, E343, and F337. The substrate-bound form is colored green (PDB entry 2HRE), and the H263C variant is colored orange. The bound protoporphyrin IX is colored red.

Overall, the structures of the three variants are as expected very similar to each other with a rmsd (Cα) ranging from 0.21 to 0.26 Å when the structures (dimers) are superimposed (*23*) with each other, and with the structure of the R115L variant [the rmsd (Cα) between the two Fc monomers comprising the 1HRK dimer is 0.16 Å]. In all cases, three cholate molecules (required for solubilization) were found in the putative active site pocket, which was observed in the R115L structure. The coordinates for the three ferrochelatase variants described in this work have been deposited in the Protein Data Bank (*24*) (see Table 1). All graphic representations were created using PYMOL (*25*) and WinCOOT (*26*).

RESULTS

Structure Determination for Variants. The crystal structure of an R115L (herein referred to as the wild type) human ferrochelatase variant was initially determined by Wu et al. (*7*) at 2.0 Å, and more recently, this has been refined to 1.7 Å by Medlock et al. (*14*). The enzyme is a homodimer with each subunit possessing a [2Fe-2S] cluster. Additionally, the structure of human ferrochelatase with the bound protoporphyrin IX substrate has been determined to 2.5 Å (*14*). In the porphyrin-bound enzyme, several active site residues possess altered spatial positions when compared to the porphyrin-free enzyme. Three of these residues, H263, F337, and H341, were selected as targets for site-directed mutagenesis in this study. The specific individual mutations were H263C, F337A, and H341C. While the H263C and H341C variants are purified with less than stoichiometric amounts of porphyrin, the crystallized proteins contained no bound porphyrin or heme. All three variant ferrochelatases crystallized (Table 1) in the same space group as the wild-type protein (*7*) and diffracted to 2.2 Å.

The structures of both H263C and H341C variant ferrochelatases can be superimposed on the R115L human ferrochelatase variant with the exception of the side chains of N75, M76, R164, H263, F337, H341, and E343 (Figure 1A). In the F337A variant ferrochelatase, the spatial orientation of all side chains is identical to that of the wild-type human ferrochelatase. Interestingly, the side chains listed above that are reoriented in the H263C and H341C variants are the same ones that have an altered spatial position in human ferrochelatase with the bound porphyrin substrate (Figure 1B). None of these side chains makes significant contact with the porphyrin macrocycle.

Table 2: Effect of Amino Acid Replacement on the Activity of Human Ferrochelatase

altered residue	K_m^{Fe} (μM)	$K_m^{porphyrin}$ (μM)	K_{cat} (min^{-1})
none	11.9	12.1	3.44
N75A	33.8	16.8	0.96
M76A	–	–	0
F337A	17.7	24.6	0.81
H263C (*15*)	–	–	0
E343D (*15*)	9.8	12.3	0.7

Kinetic Examination. Previously, we have produced and kinetically characterized R164L, H263C, H341C, E343Q, Y123F, and Y191F ferrochelatases which are discussed in this study (*15*). Additional variants produced for this study are N75A, M76A, and F337A. Kinetic data for these variants are listed in Table 2. All of the variants that were examined possessed intact [2Fe-2S] clusters and were as stable to storage as the wild-type ferrochelatase. Efforts to "rescue" the activity of an H263A mutant by inclusion of 300 mM imidazole in the assay buffer were unsuccessful (*15*).

DISCUSSION

The mechanism by which metal is inserted into a porphyrin macrocycle is relatively well understood for solution chemistry but is poorly understood for enzyme-catalyzed reactions. Insertion of iron into protoporphyrin to form heme is catalyzed by ferrochelatase, and current knowledge of this reaction is based largely upon studies of the human and *B. subtilis* enzymes. From solution studies, it was proposed that macrocycle distortion is a key feature that decreases the energy barrier for metalation. Two additional observations support this hypothesis. (i) Small ribozymes can distort

porphyrins and facilitate metalation (*27*, *28*), and (ii) antibodies raised against N-alkylated porphyrins (which themselves are bent ~30°) will bind and distort porphyrins and facilitate metalation (*29*).

The finding that *N*-methylprotoporphyrin, which has the alkylated ring bent ~35° out of the plane of the macrocycle, is a tight-binding competitive inhibitor of ferrochelatase fits the distortion model nicely as a putative transition state analogue of ferrochelatase. Crystallographic studies on the *B. subtilis* ferrochelatase with bound *N*-methylmesoporphyrin led to a number of studies and resulted in proposed models for catalysis that were based upon the assumption that this molecule was bound in the active site in a fashion identical to the position occupied by the substrate protoporphyrin. With the recent publication of human ferrochelatase with bound protoporphyrin, it is clear that *N*-methylmesoporphyrin does not occupy the same site as substrate and, therefore, cannot be considered a transition state analogue (*14*).

The structure of human ferrochelatase with the bound porphyrin substrate differs markedly from the structure of the protein without substrate bound. Most notable are the fact that the mouth of the active site is closed and a set of active site residues occupy different spatial orientations. In this study, we have produced site-directed variants for three of these residues, H263, F337, and H341, to see if any single mutation causes either a change in the spatial orientation of other active site residues or a closing of the active site mouth. During the course of site-directed mutagenesis studies, it was noted that H263A, -C, and -N ferrochelatase preparations have no enzyme activity either in vitro or in vivo and are isolated with bound protoporphyrin (*15*). Incubation overnight with ferrous iron did not result in the conversion of enzyme-bound porphyrin into heme. Crystallographic studies on H263C were carried out, and it was found that several active site residues were reoriented in the H263C variant relative to the wild-type enzyme. In the human ferrochelatase H263C variant, there is an altered orientation of the side chains of N75, M76, R164, F337, H341, and E343 (Figure 1A). No other residues in the active site or outside of the pocket were significantly altered in spatial orientation, and the active site mouth is open. Structures of the two additional active site variants, H341C and F337A, were also determined. While the F337A variant appeared to be identical to the wild type except for the replacement of the phenyl side chain, H341C had the same altered orientation of side chains that was found with H263C.

For both H263C and H341C, the alteration in the orientation of side chains is significant and essentially identical. Interestingly, the H341C mutation results in modestly decreased enzymatic activity, whereas H263C has no activity. Thus, this reorientation alone does not cause the loss of enzyme activity, but these data do suggest that a mutation causing reorientation of these active site residues may have an impact on the catalytic efficiency of the enzyme. The inactivity of the H263C variant may be attributable to the loss of this key residue and its ability to serve as a proton acceptor in the reaction (*1*). Given that cysteine should be able to serve at some level as a metal ion ligand, it might be expected that H263C should retain some activity if the role of H263 is as a metal ligand for catalysis, but this was not found to be the case.

Examination of the wild-type human structure strongly suggests that a hydrogen bonding network involving H263, H341, and E343 normally exists. The altered orientation of H341, E343, and F337 in the variants may be due to disruption of this hydrogen bond network. Disruption of this network results in the side chains of E343 and H341 rotating away from their central pocket position and thereby allowing F337, which is usually inhibited from movement by the imidazole ring of H341, to drop into the pocket.

The crystal structure of the F337A ferrochelatase variant shows that this residue does not play a direct role in the alteration of side chain orientation, as might be expected, since it does not actively participate in the hydrogen bond network. Kinetic data from the variant make it clear, however, that F337 plays a key role in catalysis (Table 2). We propose that its role is twofold. First, movement of the phenyl ring of F337 along with movement of the imidazole ring of H341 reshapes the back of the active site pocket. Second, F337 appears to act as a door that alternatively opens and closes the entrances to two solvent-filled tunnels located at the back of the active site pocket (Figure 2). The F337A variant has a small side chain, so both tunnels are open at all times. We propose that one of these solvent-filled tunnels is the entrance route for the substrate iron on the back side of the ferrochelatase molecule (*30*) and may also serve as a "rear exit" (*31*) for active site water molecules which must exit to allow space for the porphyrin macrocycle. Given that kinetic data suggest an ordered reaction with iron binding before porphyrin (*11*), this tunnel could satisfy both roles by first allowing iron into the active site pocket and then allowing water molecules an exit route as the porphyrin enters the pocket and displaces water.

On the basis of the data given above, we propose that catalysis involves the following scenario. Following iron binding within the active site, porphyrin enters the active site pocket, and at least one pyrrole proton forms a hydrogen bond with the imidazole of H263. This event triggers the catalytic cycle by disrupting the "resting state" hydrogen bond between H263 and the side chain of E343 (3.2 Å). This in turn allows E343 to reorient and shorten the previously existing hydrogen bond with the side chain of H341 from 3.4 to 2.9 Å while increasing the distance between H263 and E343 to almost 5 Å. Upon reorientation, the movement of the imidazole side chain of H341 allows the side chain ring of F337 to rotate into the pocket. H341 may now form a hydrogen bond with the hydroxyl of the phenol ring of Y123 (2.9 Å) (Figure 3A). Movement of F337 opens the entrance of a short tunnel and closes the opening of a long amphipathic, solvent-filled tunnel that extends to the surface on the backside of the molecule at H240 (Figure 2).

Reorientation of side chains also occurs on the opposite side of the active site pocket from H263. The impetus for this motion appears to involve N75 which rotates slightly. In the resting state, N75 may hydrogen bond with the hydroxyl of Y191 (3.1 Å), which in turn may hydrogen bond to the guanido group of R164 (3.4 Å). R164 can also participate in hydrogen bonds with S202 (2.6 Å) and S201 (3.3 Å) and the carbonyl group of T198. After reorientation, N75 hydrogen bonds to the backbone nitrogen of M76 (2.7 Å), allowing the side chain of M76 to rotate down into the pocket. However, the most dramatic change occurs with R164 which rotates approximately 180° out of the active

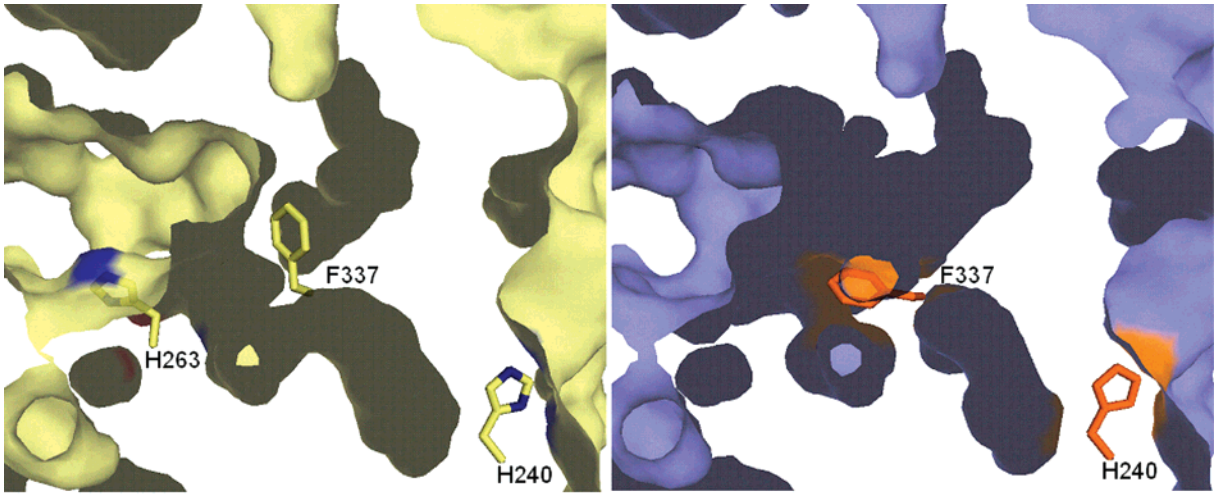

FIGURE 2: Tunnels from the protein surface to the active site. A cross section through the active site of the wild type and the H263C variant human ferrochelatases is shown. The active site opening is to the left and back. The wild-type surface is colored cream, and the H263C variant surface is colored slate. The position of the centrally located and essential H263 is shown in the wild-type structure in cream and blue for carbon and nitrogen, respectively. The figure illustrates the reorientation of the residues described in the text which result in the closing off of the tunnel opening seen at the bottom of this diagram and the opening of another tunnel entrance at the top of the picture. These alterations result mainly from the movement of the side chain of F337, shown as sticks in the middle of the diagram. The expansion of the pocket seen at the top of the diagram is attributable to the reorientation of the side chain of R164.

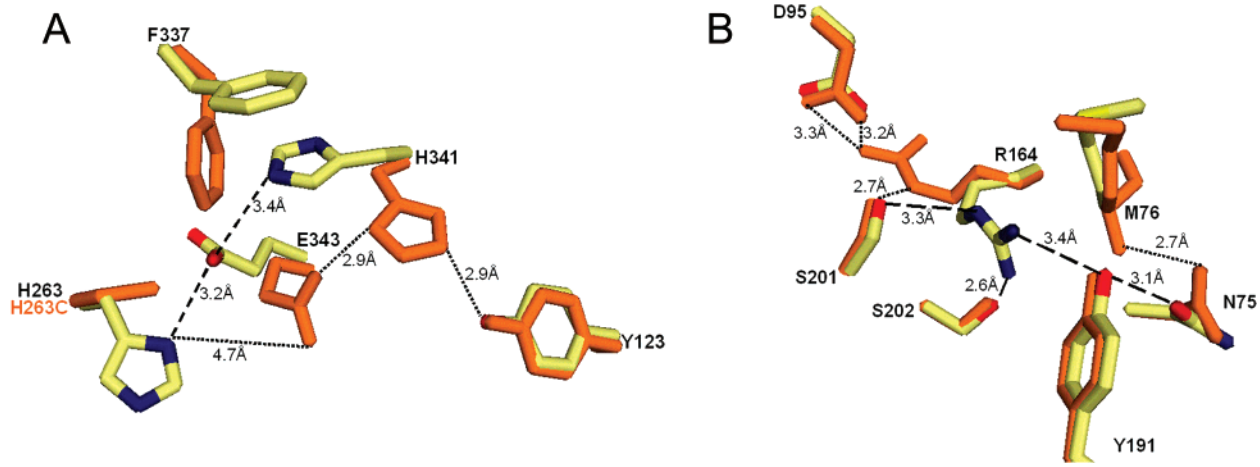

FIGURE 3: Hydrogen bonding of active site residues in the resting state and activated state of human ferrochelatase. (A) Hydrogen bonding of the bottom of the active site pocket involving H263, E343, H341, and Y123 in the resting state (– – –) and in the activated state (•••). The wild-type enzyme is colored cream, red, blue, and yellow for carbon, oxygen, nitrogen, and sulfur atoms, respectively, and the H263C variant is colored orange. (B) Hydrogen bonding of the top of the active site pocket involving N75, M76, D95, R164, Y191, S201, and S202 in the resting state (– – –) and in the activated state (•••). The wild-type enzyme is colored cream, red, blue, and yellow for carbon, oxygen, nitrogen, and sulfur atoms, respectively, and the H263C variant is colored orange.

site pocket. Its new position is stabilized by hydrogen bonds between the guanido group of R164, the hydroxyl group of S201 (2.7 Å), and the carboxylate group of D95 (3.2 and 3.3 Å) (Figure 3B). The movement of R164 creates a pocket over the center of the porphyrin macrocycle adjacent to the side chain of M76. The ultimate impact of these rearrangements is the remodeling of the active site pocket in such a manner that could result in distortion of the porphyrin macrocycle which would facilitate iron insertion (Figure 4). Mutagenesis and characterization of N75, M76, E343, H341, F337, Y191, Y123, and R164 yielded kinetic data that are consistent with this proposal (Table 2) (*15*).

The weakened catalytic ability of N75A is of interest since the amide side chain of asparagine has little impact on the shape of the active site pocket, and its minor movement from the wild type to H263C or H341C does not spatially alter the active site pocket. It does, however, appear to be key to the hydrogen bond network connecting the H263 side of the pocket with the R164 side. The side chain of M76 protrudes slightly downward into the pocket over one of the pyrrole rings of the macrocycle (Figure 4). An M76A variant eliminates this physical presence and thereby may allow sufficient movement of the porphyrin macrocycle to prevent ring distortion or optimal orientation for metal insertion.

To end the catalytic cycle, insertion of metal into the porphyrin nucleus will release H263 to re-create the hydrogen bond network via interaction with E343. Such an event would alter the geometry of the active site, allowing release of the heme, which may be facilitated by movement of the guanido group of R164 back down over the now metalated product, thereby creating charge repulsion between the iron in heme and the guanido group of R164. Rotation of F337 reopens the amphipathic tunnel, thereby allowing water to move back into the active site pocket as the heme exits.

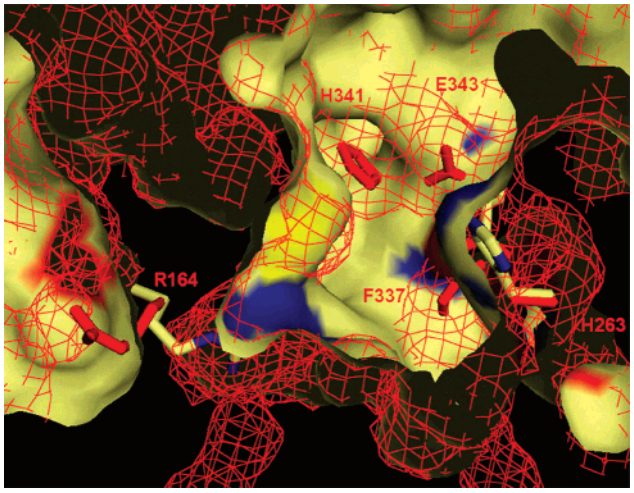

FIGURE 4: Remodeling of the active site pocket. A segment through the active site is shown with a surface representation of the wild-type ferrochelatase colored cream. The H263C variant surface is shown as a red mesh. The R164 residue is to the left and reorients outward to the surface in the variant. H341 and E343 of the variant can be seen to reorient into the active site pocket. F337 of the variant moves into the bottom right of the active site as shown here. M76 rotates slightly, and its mesh-represented density can be seen near the center of the active site.

Since the active site remains open despite significant changes in positions of specific side chains, it is clear that something other than re-formation of the hydrogen bond network must trigger or cause the active site mouth to close. The impetus for this may be hydrophobic interactions between the macrocycle and aromatic active site residues or interactions between the porphyrin propionates and polar residues.

It is of interest that many of the active site residues that are discussed above are not conserved among all ferrochelatases. Indeed, H263, Y123, F337, and E343 are the only conserved residues discussed in this study, and all of these are located on one surface of the active site. Examination of available structures and modeling of other ferrochelatases using threader programs clearly demonstrate that while the overall catalytic function of ferrochelatases may be conserved, the exact residues playing catalytic roles vary considerably. However, these data support a catalytic model for human ferrochelatase in which initial porphyrin substrate binding triggers a cascade of hydrogen bond realignments that result in reshaping of the active site and distortion of the macrocycle, thereby facilitating iron insertion.

REFERENCES

1. Dailey, H. A., and Dailey, T. A. (2003) Ferrochelatase, in *The Porphyrin Handbook* (Kadish, K. M., Smith, K. M., and Guilard, R., Eds.) pp 93−121, Academic Press, New York.
2. Goldberg, A., Ashenbrucker, H., Cartwright, G. E., and Wintrobe, M. M. (1956) Studies on the Biosynthesis of Heme In Vitro by Avian Erythrocytes, *Blood 11*, 821−833.
3. Dailey, H. A., Dailey, T. A., Wu, C. K., Medlock, A. E., Wang, K. F., Rose, J. P., and Wang, B. C. (2000) Ferrochelatase at the millennium: Structures, mechanisms and [2Fe-2S] clusters, *Cell. Mol. Life Sci. 57*, 1909−1926.
4. Dailey, T. A., and Dailey, H. A. (2002) Identification of [2Fe-2S] clusters in microbial ferrochelatases, *J. Bacteriol. 184*, 2460−2464.
5. Al-Karadaghi, S., Hansson, M., Nikonov, S., Jonsson, B., and Hederstedt, L. (1997) Crystal structure of ferrochelatase: The terminal enzyme in heme biosynthesis, *Structure 5*, 1501−1510.
6. Karlberg, T., Lecerof, D., Gora, M., Silvegren, G., Labbe-Bois, R., Hansson, M., and Al-Karadaghi, S. (2002) Metal binding to *Saccharomyces cerevisiae* ferrochelatase, *Biochemistry 41*, 13499−13506.
7. Wu, C. K., Dailey, H. A., Rose, J. P., Burden, A., Sellers, V. M., and Wang, B. C. (2001) The 2.0 Å structure of human ferrochelatase, the terminal enzyme of heme biosynthesis, *Nat. Struct. Biol. 8*, 156−160.
8. Dailey, H. A., Finnegan, M. G., and Johnson, M. K. (1994) Human ferrochelatase is an iron-sulfur protein, *Biochemistry 33*, 403−407.
9. Shepherd, M., Dailey, T. A., and Dailey, H. A. (2006) A new class of [2Fe-2S]-cluster-containing protoporphyrin (IX) ferrochelatases, *Biochem. J. 397*, 47−52.
10. Lecerof, D., Fodje, M. N., Alvarez Leon, R., Olsson, U., Hansson, A., Sigfridsson, E., Ryde, U., Hansson, M., and Al-Karadaghi, S. (2003) Metal binding to *Bacillus subtilis* ferrochelatase and interaction between metal sites, *J. Biol. Inorg. Chem. 8*, 452−458.
11. Dailey, H. A., and Fleming, J. E. (1983) Bovine ferrochelatase. Kinetic analysis of inhibition by N-methylprotoporphyrin, manganese, and heme, *J. Biol. Chem. 258*, 11453−11459.
12. Lecerof, D., Fodje, M., Hansson, A., Hansson, M., and Al-Karadaghi, S. (2000) Structural and mechanistic basis of porphyrin metallation by ferrochelatase, *J. Mol. Biol. 297*, 221−232.
13. Hansson, M. D., Karlberg, T., Rahardja, M. A., Al-Karadaghi, S., and Hansson, M. (2007) Amino Acid Residues His183 and Glu264 in *Bacillus subtilis* Ferrochelatase Direct and Facilitate the Insertion of Metal Ion into Protoporphyrin IX, *Biochemistry 46*, 87−94.
14. Medlock, A., Swartz, L., Dailey, T. A., Dailey, H. A., and Lanzilotta, W. N. (2007) Substrate Interactions with Human Ferrochelatase, *Proc. Natl. Acad. Sci. U.S.A. 104*, 1789−1793.
15. Sellers, V. M., Wu, C. K., Dailey, T. A., and Dailey, H. A. (2001) Human ferrochelatase: Characterization of substrate-iron binding and proton-abstracting residues, *Biochemistry 40*, 9821−9827.
16. Burden, A. E., Wu, C., Dailey, T. A., Busch, J. L., Dhawan, I. K., Rose, J. P., Wang, B., and Dailey, H. A. (1999) Human ferrochelatase: Crystallization, characterization of the [2Fe-2S] cluster and determination that the enzyme is a homodimer, *Biochim. Biophys. Acta 1435*, 191−197.
17. Najahi-Missaoui, W., and Dailey, H. A. (2005) Production and characterization of erythropoietic protoporphyric heterodimeric ferrochelatases, *Blood 106*, 1098−1104.
18. Teng, T. Y. (1990) Mounting of crystals for macromolecular crystallography in a freestanding thin-film, *J. Appl. Crystallogr. 23*, 387−391.
19. Otwinowski, Z., and Minor, W. (1997) Processing of X-ray diffraction data collected in oscillation mode, *Methods Enzymol. A276*, 307−326.
20. Brunger, A. T., Adams, P. D., Clore, G. M., DeLano, W. L., Gros, P., Grosse-Kunstleve, R. W., Jiang, J. S., Kuszewski, J., Nilges, M., Pannu, N. S., Read, R. J., Rice, L. M., Simonson, T., and Warren, G. L. (1998) Crystallography & NMR system: A new software suite for macromolecular structure determination, *Acta Crystallogr. D54*, 905−921.
21. Murshudov, G. N., Vagin, A. A., and Dodson, E. J. (1997) Refinement of macromolecular structures by the maximum-likelihood method, *Acta Crystallogr. D53*, 240−255.
22. McRee, D. E. (1999) XtalView/Xfit: A versatile program for manipulating atomic coordinates and electron density, *J. Struct. Biol. 125*, 156−165.
23. Huang, C. C., Couch, G. S., Pettersen, E. F., and Ferrin, T. E. (1996) Chimera: An Extensible Molecular Modeling Application Constructed Using Standard Components, *Pac. Symp. Biocomput. '99*, 724.
24. Berman, H. M., Battistuz, T., Bhat, T. N., Bluhm, W. F., Bourne, P. E., Burkhardt, K., Feng, Z., Gilliland, G. L., Iype, L., Jain, S., Fagan, P., Marvin, J., Padilla, D., Ravichandran, V., Schneider, B., Thanki, N., Weissig, H., Westbrook, J. D., and Zardecki, C. (2002) The Protein Data Bank, *Acta Crystallogr. D58*, 899−907.

25. DeLano, W. L. (2002) *The PyMOL Molecular Graphics System*, 0.99 ed., DeLano Scientific, San Carlos, CA.
26. Emsley, P., and Cowtan, K. (2004) Coot: Model-building tools for molecular graphics, *Acta Crystallogr. D60*, 2126−2132.
27. Li, Y., and Sen, D. (1997) Toward an efficient DNAzyme, *Biochemistry 36*, 5589−5599.
28. Conn, M. M., Prudent, J. R., and Schultz, P. G. (1996) Porphyrin Metalation Catalyzed by a Small RNA Molecule *J. Am. Chem. Soc. 118*, 7012−7013.
29. Cochran, A. G., and Schultz, P. G. (1990) Antibody-catalyzed porphyrin metallation, *Science 249*, 781−783.
30. Lange, H., Kispal, G., and Lill, R. (1999) Mechanism of iron transport to the site of heme synthesis inside yeast mitochondria, *J. Biol. Chem. 274*, 18989−18996.
31. Meyer, E. (1992) Internal water molecules and H-bonding in biological macromolecules: A review of structural features with functional implications, *Protein Sci. 1*, 1543−1562.
32. Laskowski, R. A., MacArthur, M. W., Moss, D. S., and Thornton, J. M. (1993) PROCHECK: A program to check the stereochemical quality of protein structures, *J. Appl. Crystallogr. 26*, 283−291.

BI700151F